LA-UR-21-20856
Approved for public release; distribution is unlimited.

Title: Enskog Transport Calculations with Magpie

Author(s): Velizhanin, Kirill A.

Intended for: Report

Issued: 2021-02-01

Enskog Transport Calculations with Magpie

Kirill A. Velizhanin, T-1*

(Dated: 01/28/21)

The revised Enskog theory for mixtures has been implemented, as a library, in the LANL institutional thermochemical code Magpie. This report provides the necessary physical background and several representative examples of transport calculations with this library. The particular attention is paid to how the contributions of non-translational degrees of freedom (molecular vibrations, rotations, electronic excitations) to the energy transport can be consistently accounted for via the so called Eucken correction.

I. INTRODUCTION

Magpie is a Python-based LANL thermochemical code/library with one of the main capabilities being evaluation of a thermodynamically complete equation of state (EOS) of a dense mixture of gases/fluids subject to chemical equilibration [14]. The EOS of the mixture is evaluated using the Ross variational perturbation theory [13], where an effective hard sphere diameter of molecules of each chemical species in the mixture is evaluated as a by-product. In certain applications, the EOS needs to be supplemented with transport properties of the mixture, e.g., thermal conductivity or viscosity. The Chapman-Enskog and Enskog theories can be suitable for this [2]. The former theory relies on the exact intermolecular interaction potential and is, therefore, expected to be very accurate within the domain of its applicability. However, it is only applicable at low densities where the mean free path is much larger than the molecular diameter which makes this theory inapplicable for dense mixtures. Another complication is that in mixtures the number of parameters to describe the intermolecular potentials grows quadratically with the number of chemical species and such parameters are rarely available. On the other hand, the Enskog theory is based on approximating the repulsive part of intermolecular potentials by that of hard spheres and neglecting the attraction part. The Enskog theory's formulae is applicable at arbitrary densities, and the hard sphere diameters, required for evaluation of collision integrals, can by provided by the Ross perturbation theory, as implemented in Magpie. Since the intermolecular attraction is neglected and the repulsion assumed very sharp (i.e., hard spheres), the Enskog theory is expected to be accurate for either highly compressed mixtures (packing fraction ~ 1) at arbitrary temperatures, or for mixtures of arbitrary density at temperatures significantly higher than the critical temperature.

We have implemented the Enskog theory in Magpie as a library, i.e., a set of functions that evaluate transport coefficients and some auxiliary thermodynamic quantities. This report provides the physical background and illustrative examples for how the Enskog theory can be used to calculate the transport properties of mixtures. This is not a manual in a sense that it does not provide information about what functions to call and with what input arguments. The main focus of this report turned out to be how to correctly account for the non-translational degrees of freedom of a molecule (e.g., vibrations, rotations) when evaluating the energy flux and related quantities. The "pure" Enskog theory, as for example described and used in Refs. [4, 9], does not deal with the non-translational degrees of freedom, so the so called Eucken correction [5] is introduced, described and illustrated by several examples in this work. Some of the transport properties are unaffected by the non-translational degrees of freedom under the approximations specific to the Eucken correction. This is the reason why, for example, the viscosity - an important transport property - is discussed only briefly here.

The report is organized as follows. Overview of the general theory is given in Sec. II, where a particular attention is paid to how to describe transport in a regime where fast chemical equilibration is present, Sec. II A. The "pure" Enskog theory and how to modify it to account for the non-translational (or intra-molecular) degrees of freedom is described in Sec. III. Illustrative examples are provided and discussed in Sec. A. Sec. V concludes.

* kirill@lanl.gov

II. GENERAL THEORY OF IRREVERSIBLE PROCESSES IN HYDRODYNAMICS

The Euler equations for the specific (i.e., per unit mass) internal energy and density of species i within a mixture are

$$\dot{e} = -\frac{P}{\rho}\left(\nabla \cdot u\right), \tag{1}$$

$$\dot{\rho}_i = -\rho_i\left(\nabla \cdot u\right), \tag{2}$$

where $i = 1, 2, \ldots, N$ (N is the number of chemical species), the dot above variables denotes the material time derivative, P is the pressure and $\rho = \sum_i \rho_i$ is the total density. The center of mass particle velocity u is defined by $\rho u = \sum_i \rho_i u_i$, where u_i is the flow velocity of species i. Adding such irreversible processes as energy and material transport, as well as chemical transformations results in the following equations [3]

$$\dot{e} = -\frac{P}{\rho}\left(\nabla \cdot u\right) - \frac{1}{\rho}\left(\nabla \cdot J_e\right), \tag{3}$$

$$\dot{\rho}_i = -\rho_i\left(\nabla \cdot u\right) - \left(\nabla \cdot J_i\right) + R_i(\{\rho\}, e), \tag{4}$$

where J_e is the energy flux (energy per unit area per unit time), and $J_i = \rho_i(u_i - u)$ is the material flux of species i defined relative to the center of mass movement (mass per unit area per unit time). Notation for the set of all the densities is $\{\rho\} = \{\rho_i | i = 1, 2, \ldots, N\}$. Pressure is given by the EOS as $P = P(\{\rho\}, e)$. The rate of chemical transformations is given by R_i (density per unit time). The mass conservation and the definition of J_i imply $\sum_i R_i = 0$ and $\sum_i J_i = 0$, respectively. We further assume that deviations from equilibrium with respect to mass and energy fluxes are not large, so we can write the fluxes using the linear transport coefficients as [3]

$$J_i = \sum_j L_{ij} X_j + L_{ie} X_e,$$

$$J_e = \sum_i L_{ei} X_i + L_{ee} X_e, \tag{5}$$

where the transport "forces" are defined as

$$X_i = -T\nabla(\mu_i/T), \tag{6}$$

$$X_e = -T^{-1}\nabla T, \tag{7}$$

where T is the temperature. The chemical potential μ_i of species i is introduced via the exact differential for the extensive internal energy $dE = TdS - PdV + \sum_i \mu_i dM_i$, where M_i is the total mass of species i in the system. This definition of the chemical potential, typical in transport literature, is different from the one given by the standard extensive expression $dE = TdS - PdV + \sum_i \mu_i^{(c)} dN_i$ typically used in physical chemistry, where N_i is the total extensive number of molecules in the system. The relation between the two is then $\mu_i = \mu_i^{(c)}/m_i$, where m_i is the mass of the single molecule of species i.

The choice of the forces, Eqs. (6) and (7), is not unique. For example, X_i could be chosen to be proportional to the gradient of concentration. The specific choice of the forces here is motivated by the Onsager theory of reciprocal relations [3, 12], which can be used to demonstrate that the transport coefficients are symmetric, $L_{ij} = L_{ji}$ and $L_{ei} = L_{ie}$, for the choice of forces given by Eqs. (6) and (7). Other matrix properties, $\sum_i L_{ij} = 0$ and $\sum_i L_{ie} = 0$, follow from $\sum_i J_i = 0$. In particular, this implies that L_{11} and L_{1e} vanish for a mono-component gas/fluid.

It is instructive to use Eqs. (3) and (4) to calculate the material derivative of specific entropy. To this end, we re-write the exact extensive differential $dE = TdS - PdV + \sum_i \mu_i dM_i$ as

$$Tds = de - \frac{P}{\rho^2} d\rho - \sum_i \mu_i d\left(\frac{\rho_i}{\rho}\right). \tag{8}$$

Substituting Eqs. (3) and (4) into this equation we obtain

$$T\dot{s} = -\frac{1}{\rho}\left(\nabla \cdot J_e\right) + \sum_i \frac{\mu_i}{\rho}\left(\nabla \cdot J_i\right) - \sum_i \frac{\mu_i}{\rho} R_i. \tag{9}$$

Further, using Eqs. (5) and (7) produces

$$\rho\dot{s} = -\nabla\cdot\left(\frac{J_e - \sum_i \mu_i J_i}{T}\right) + \frac{X_e J_e + \sum_i X_i J_i}{T} - \frac{1}{T}\sum_i \mu_i R_i. \tag{10}$$

Entropy change in the unit volume, $\rho\dot{s}$, is thus given by the divergence of the "entropy flux", the first r.h.s. term, and the spatially local production of entropy due to (i) energy and mass transport, the second r.h.s. term, as well as (ii) chemical transformations, the third r.h.s. term. The last two terms must be positive semi-definite according to the second law of thermodynamics, which for mass/energy transport implies that the matrix

$$\begin{bmatrix} L_{ee} & L_{e1} & \dots & L_{eN} \\ L_{1e} & L_{11} & \dots & L_{1N} \\ \vdots & \vdots & \ddots & \vdots \\ L_{Ne} & L_{N1} & \dots & L_{NN} \end{bmatrix} \tag{11}$$

is positive semi-definite. Chemical reactions always proceed in the direction of decreasing Gibbs free energy at constant P and T, so that $dg = \sum_i \mu_i R_i \leq 0$, and so the last term term in Eq. (10) is strictly non-negative. That the evolution of entropy in Eq. (10) is governed only by J_i, J_e and R_i, and not by general hydrodynamic evolution coming from Eq. (2), explains why the corresponding processes of the mass/energy transport and chemical transformations are referred to as irreversible here.

A. Fast Chemical Equilibration

An important limiting case is when the timescale of local chemical equilibration $\tau_{chem} \propto R_i^{-1}$ is significantly shorter than the fastest of the hydrodynamic and energy/mass transport timescales τ_*. For any local state ($\{\rho\}$, e) it is convenient to introduce $\tilde{\rho}_i(\{\rho\}, e)$ - the density resulting from chemical equilibration of an isolated system (i.e., no energy or mass flows) of constant volume subject to elemental densities fixed by $\{\rho\}$. What is implied here is that chemical transformations, determined by R_i, are assumed ergodic on the timescale τ_{chem}. It might not be the case when the considered $\{R_i\}$ do constitute a thermodynamically complete set of transformations, or some transformations are slow. We only consider chemical transformations that are ergodic in this work.

We consider integration of Eqs. (3) and (4) over the time step Δt chosen so that $\tau_{chem} \ll \Delta t \ll \tau_*$. The integration is performed in two steps in the first-order operator splitting manner where, first, Eqs. (3) and (4) are evolved over Δt with R_i set to zero, and then only chemical reactions are propagated over Δt in a cell of constant internal energy and volume, with no mass transport. The initial state before the integration step is $e(t)$ and $\{\rho(t)\}$, where the density is assumed "equilibrated", i.e., $\rho_i(t) = \tilde{\rho}_i(\{\rho(t)\}, e(t))$. Upon the first step, the energy and density change by

$$\Delta_1 e = -\frac{P}{\rho}\left(\nabla\cdot u\right)\Delta t - \frac{1}{\rho}\left(\nabla\cdot J_e\right)\Delta t, \tag{12}$$

$$\Delta_1 \rho_i = -\rho_i\left(\nabla\cdot u\right)\Delta t - \left(\nabla\cdot J_i\right)\Delta t. \tag{13}$$

The second step does not change internal energy, but transforms the density $\rho_i(t) + \Delta_1\rho_i$ to

$$\rho_i(t+\Delta t) = \tilde{\rho}_i(\{\rho(t) + \Delta_1\rho\}, e(t) + \Delta_1 e) \approx \sum_j \frac{\partial\tilde{\rho}_i}{\partial\rho_j}\Delta_1\rho_j + \frac{\partial\tilde{\rho}_i}{\partial e}\Delta_1 e, \tag{14}$$

where all the partial derivatives of $\tilde{\rho}_i$ are evaluated at the state $\{\rho(t)\}$, e. Combining the results of the two steps, Eqs. (3) and (4) become

$$\dot{e} = -\frac{P}{\rho}\left(\nabla\cdot u\right) - \frac{1}{\rho}\left(\nabla\cdot J_e\right), \tag{15}$$

$$\dot{\rho}_i = \sum_j \frac{\partial\tilde{\rho}_i}{\partial\rho_j}\left[-\rho_j\left(\nabla\cdot u\right) - \left(\nabla\cdot J_j\right)\right] + \frac{\partial\tilde{\rho}_i}{\partial e}\dot{e}. \tag{16}$$

What this result physically means is that to describe the situation with the very fast chemical equilibration, one can still use Eqs. (3) and (4) with R_i set to zero, but the resulting $\rho_i(t)$ must not be taken literally. Instead, $\{\rho(t)\}$ just fixes the elemental densities and the actual density is given by $\tilde{\rho}_i(\{\rho(t)\}, e)$, and this is this last density that has to be used to calculate transport fluxes J_i, J_e, as well as the pressure.

We now use the same approach for the entropy evolution. The first step of the operator splitting approach yields

$$\rho\Delta_1 s = -\nabla\cdot\left(\frac{J_e-\sum_i \mu_i J_i}{T}\right)\Delta t + \frac{X_e J_e+\sum_i X_i J_i}{T}\Delta t. \tag{17}$$

The second step corresponds to the local entropy production due to chemical transformations at constant internal energy

$$\Delta_2 s = s\left(\{\tilde{\rho}\left(\{\rho+\Delta_1\rho\},\epsilon+\Delta_1\epsilon\right)\},\epsilon+\Delta_1\epsilon\right) - s(\{\rho+\Delta_1\rho\},\epsilon+\Delta_1\epsilon). \tag{18}$$

Since $\tilde{\rho}_i(\{\rho\},e)$ effectively produces the full chemical equilibration of $\{\rho\}$, then $s(\{\rho\},e)$, as a function of $\{\rho\}$, reaches its maximum at $\tilde{\rho}(\{\rho\},e)$ subject to the elemental densities constrained by $\{\rho\}$. It is then straightforward to show using the two-variable Taylor expansion and that $\rho_i(t)$ is equilibrated (i.e., $\rho_i(t)=\tilde{\rho}_i(\{\rho(t)\},e(t))$, that

$$\tilde{\rho}\left(\{\rho(t)+\Delta_1\rho\},e(t)+\Delta_1 e\right) = \rho(t)+O(\Delta t). \tag{19}$$

Since $s\left(\{\tilde{\rho}\left(\{\rho+\Delta_1\rho\},\epsilon+\Delta_1\epsilon\right)\},\epsilon+\Delta_1\epsilon\right)$ is the entropy's maximum, we have $\Delta_2 s = O(\Delta t^2)$, and therefore it can be neglected compared to $\Delta_1 s$. Therefore, the entropy evolution can just be calculated with Eq. (10) with the last term omitted. It could be more complicated when the chemical reaction does not lead to complete equilibration (i.e., non-ergodic), that is when the large-time asymptotic solution of $\dot{\rho'}_i = R_i(\{\rho'\},e)$ with the initial density $\{\rho\}$ does not produce $\tilde{\rho}_i(\{\rho\},e)$.

III. ENSKOG THEORY

The Enskog theory is an approximate method for evaluating transport coefficients for a gas/fluid of hard spheres [2, 5]. In Magpie we have implemented the so called revised Enskog theory (RET) for mixtures [9], where "mixtures" stands for the gas/fluid composed of multiple hard-sphere species (each specified by the diameter and mass of a hard-sphere, and the concentration), and "revised" means that this version of the multi-component Enskog theory preserves the symmetry of the Onsager coefficients, unlike some earlier attempts.

With regards to the notation and quantities to be calculated, we most closely follow Ref. [4]. Specifically, the Magpie-based implementation of RET allows one to evaluate transport coefficients $L_{ij}^{(E)}$, $L_{ie}^{(E)}$, $L_{ee}^{(E)}$, $D_i^{(E)}$ and $\eta^{(E)}$, where the first three transport coefficients were introduced above, the self-diffusion coefficient $D_i^{(E)}$ will be introduced in what follows, and $\eta^{(E)}$ is the dynamic viscosity. The superscript "(E)" stands for Enskog. The reason we explicitly have this superscript is that since the Enskog theory has been developed for hard spheres, it does not describe the energy transport due to the internal degrees of freedom (iDOF), which include rotations, vibrations and electronic excitations. Therefore, RET has to be modified when dealing with molecules, as well as atoms if electronic excitations are deemed important. This can be done approximately by treating the collision between the molecules as independent of the specific iDOF state, i.e., (i) the probability of energy exchange between the iDOFs of a pair of colliding molecules is assumed small during a single collision, and (ii) collision integrals are only weakly dependent on the specific energy accumulated in iDOFs . In what follows we relate the Enskog transport coefficients to the "full" ones using the approach where molecules of the same chemical species, but in different quantum states with regard to iDOFs are now considered separate species [5, 7]. These new species are indexed by greek letters α, β in what follows. On the other hand, latin indices i, j enumerate chemical spices without the regard of the quantum state. Then, function $c(\alpha)$ denotes the chemical species (hence "c") to which new species α belongs. Accordingly, the mass and energy fluxes can be written as [5]

$$J_\alpha = \sum_\beta L_{\alpha\beta}^{(E)} X_\beta^{(E)} + L_{\alpha e}^{(E)} X_e, \tag{20}$$

$$J_e = \sum_\alpha L_{e\alpha}^{(E)} X_\alpha^{(E)} + \sum_\alpha L_{ee}^{(E)} X_e + \sum_\alpha \epsilon_\alpha J_\alpha, \tag{21}$$

where ϵ_α is the iDOF energy of the unit mass of species α. The Enskog mass force is defined as $X_\alpha^{(E)} = -T\nabla\left(\frac{\mu_\alpha^{(tr)}}{T}\right)$, where $\mu_\alpha^{(tr)}$ is the translational chemical potential (not the full one!) for the species α. For example, this translational chemical potential can be calculated from the Carnahan-Starling EOS [4, 10] in the case of the Enskog mixture theory, or directly from Magpie. The goal here is to convert these expressions to the form where the summations with respect

to specific quantum states are substituted with summations over chemical species. First, one can show combinatorially that the chemical potential for molecules in state α is

$$\mu_\alpha^{(tr)} = \mu_{c(\alpha)}^{(tr)} + \frac{k_B T}{m_{c(\alpha)}} \ln \frac{\rho_\alpha}{\rho_{c(\alpha)}}, \tag{22}$$

where $\rho_{c(\alpha)} = \sum_{\beta \in c(\alpha)} \rho_\beta$ is the density of chemical species of the sort index α points to. Notation $\beta \in c(\alpha)$ means the set of all β that correspond to the same chemical species α belongs to, i.e., going over all β that satisfy $c(\beta) = c(\alpha)$. Mass of a single molecule of chemical species i is denoted by m_i. Chemical potential $\mu_i^{(tr)}$ is the translational chemical potential of chemical species i as if they are all in the same quantum state. With this chemical potential, the mass force reads as

$$X_\alpha^{(E)} = -T\nabla\left(\frac{\mu_\alpha^{(tr)}}{T}\right) = -T\nabla\left(\frac{\mu_{c(\alpha)}^{(tr)}}{T} + \frac{k_B}{m_{c(\alpha)}} \ln \frac{\rho_\alpha}{\rho_{c(\alpha)}}\right) = X_{c(\alpha)}^{(E)} - \frac{k_B T}{m_{c(\alpha)}}\left(\frac{\nabla\rho_\alpha}{\rho_\alpha} - \frac{\nabla\rho_{c(\alpha)}}{\rho_{c(\alpha)}}\right). \tag{23}$$

The relation between ρ_α and $\rho_{c(\alpha)}$ is determined by the the local temperature, $\rho_\alpha = p_\alpha(T)\rho_{i(\alpha)}$, where $\sum_{\alpha\in i} p_\alpha = 1$. This assumes that equilibration over iDOF states is very fast. Using this expression, we have

$$\frac{\nabla\rho_\alpha}{\rho_\alpha} = \frac{\nabla p_\alpha}{p_\alpha} + \frac{\nabla\rho_{c(\alpha)}}{\rho_{c(\alpha)}}, \tag{24}$$

so that

$$X_\alpha^{(E)} = X_{c(\alpha)}^{(E)} - \frac{k_B T}{m_{c(\alpha)}} \frac{\nabla p_\alpha}{p_\alpha}. \tag{25}$$

The expression for the energy flux becomes

$$J_e = \sum_\alpha L_{e\alpha}^{(E)} \left[X_{c(\alpha)}^{(E)} - \frac{k_B T}{m_{c(\alpha)}} \frac{\nabla p_\alpha}{p_\alpha}\right] + \sum_\alpha L_{ee}^{(E)} X_e + \sum_\alpha \epsilon_\alpha \left\{\sum_\beta L_{\alpha\beta}^{(E)} \left[X_{c(\beta)}^{(E)} - \frac{k_B T}{m_{c(\beta)}} \frac{\nabla p_\beta}{p_\beta}\right] + L_{\alpha e}^{(E)} X_e\right\}. \tag{26}$$

To proceed further we use the relations between $L_{e\alpha}^{(E)}$, $L_{\alpha\beta}^{(E)}$ and $L_{ei}^{(E)}$, $L_{ij}^{(E)}$, obtained in App. A. The result is

$$J_e = \sum_i \left[L_{ei}^{(E)} + \sum_j \epsilon_j L_{ji}^{(E)}\right] X_i^{(E)} + \left[L_{ee}^{(E)} + \sum_i \epsilon_i L_{ie}^{(E)} + T\sum_i c_i D_i^{(E)} \rho_i\right] X_e, \tag{27}$$

where $\epsilon_i = \sum_{\alpha\in i} p_\alpha \epsilon_\alpha$ is the average iDOF energy, and $c_i = \frac{d\epsilon_i}{dT}$ is the corresponding heat capacity. The self-diffusion coefficient of chemical species i, evaluated with RET as described in App. A, is denoted by $D_i^{(E)}$. In another form, Eq. (27) could also be written as

$$J_e = J_e^{(E)} + \sum_i \epsilon_i J_i^{(E)} + T\sum_i c_i D_i^{(E)} \rho_i X_e. \tag{28}$$

Applying the transformations above to Eq. (20) converts it to

$$J_i = \sum_j L_{ij}^{(E)} X_j^{(E)} + L_{ie}^{(E)} X_e, \tag{29}$$

which means that $J_i = J_i^{(E)}$. This result is of course expected since separating species into subspecies with no difference in collisional properties does not affect the mass transport. The self-diffusion is not affected by iDOF for the same reason, so $D_i = D_i^{(E)}$. Finally, it also does not affect momentum transfer, so the viscosity is not changed by accounting for iDOF resulting in $\eta = \eta^{(E)}$. In what follows, whenever a "full" and "pure Enskog" quantities are physically the same, the superscript (E) will be omitted, for example we will not use $D_i^{(E)}$ below even though this value will be obtained directly from the pure Enskog calculations, since $D_i = D_i^{(E)}$. In fact, this convention has already been used above by not introducing $X_e^{(E)}$, since obviously $X_e = X_e^{(E)}$.

A. Entropy production

To write down the entropy balance equation we use Eq. (9) but with R_i omitted (as has to be done when the local chemical equilibration is fast), with the energy flux given by Eq. (27), and chemical potential modified by accounting for iDOF

$$\mu_i = \mu_i^{(tr)} + \epsilon_i - Ts_i, \tag{30}$$

where $s_i = \sum_{\alpha\in i} p_\alpha s_\alpha$ is the average iDOF entropy. The result is

$$\rho\dot{s} = -\frac{1}{T}\nabla\cdot\left[J_e^{(E)} + \sum_i \epsilon_i J_i^{(E)} + T\sum_i c_i D_i \rho_i X_e\right] + \sum_i \frac{\mu_i^{(tr)} + \epsilon_i - Ts_i}{T}\left(\nabla\cdot J_i^{(E)}\right). \tag{31}$$

The series of elementary (but somewhat tedious) transformations, using identities $\nabla(\epsilon_i/T) = (\epsilon_i/T - c_i)X_e$ and $c_i = \frac{d\epsilon_i}{dT} = T\frac{ds_i}{dT}$, results in

$$\rho\dot{s} = -\nabla\cdot\left[\frac{J_e - \sum_i \mu_i J_i^{(E)}}{T}\right] + \frac{X_e J_e^{(E)} + \sum_i X_i^{(E)} J_i^{(E)} + T\sum_i c_i D_i \rho_i X_e^2}{T}, \tag{32}$$

where J_e in the first term is indeed the full J_e, and not just $J_e^{(E)}$. An important observation here is that the local production, i.e., the second r.h.s. term, is strictly non-negative. This is good because it means that the Eucken correction does not break the physical consistency of the RET.

B. Full forces

Eqs. (27) and (29) are not of the form (5), where the contribution of X_e to J_i and that of X_i to J_e do have the same transport coefficient due to the Onsager symmetry. To restore that symmetry, one needs to introduce the mass force based not on the "translational" chemical potential, but on the full one, given by Eq. (30). To this end, we substitute Eq. (30) into Eq. (6) to produce the full mass force as

$$X_i = X_i^{(E)} - \epsilon_i X_e. \tag{33}$$

Using this full force allows one to rewrite Eqs. (29) and (27) as

$$J_i = \sum_j L_{ij}^{(E)} X_j + \left[L_{ie}^{(E)} + \sum_j \epsilon_j L_{ji}^{(E)}\right] X_e, \tag{34}$$

$$J_e = \sum_i \left[L_{ei}^{(E)} + \sum_j \epsilon_j L_{ji}^{(E)}\right] X_i + \left[L_{ee}^{(E)} + 2\sum_i \epsilon_i L_{ie}^{(E)} + \sum_{ij} \epsilon_i\epsilon_j L_{ij}^{(E)} + T\sum_i c_i D_i^{(E)} \rho_i\right] X_e. \tag{35}$$

The full transport coefficients thus become

$$L_{ij} = L_{ij}^{(E)}, \tag{36}$$

$$L_{ie} = L_{ei} = L_{ie}^{(E)} + \sum_j \epsilon_j L_{ji}^{(E)}, \tag{37}$$

$$L_{ee} = L_{ee}^{(E)} + 2\sum_i \epsilon_i L_{ie}^{(E)} + \sum_{ij} \epsilon_i\epsilon_j L_{ij}^{(E)} + T\sum_i c_i D_i^{(E)} \rho_i. \tag{38}$$

Importantly, the new cross coefficient $L_{ie} = L_{ie}^{(E)} + \sum_j \epsilon_j L_{ji}^{(E)}$ is the same in the both equations for J_i and J_e, and $L_{ij} = L_{ji}$. This means that the adopted approximation for the iDOF contribution to the energy transfer - the Eucken correction - is internally consistent in a sense that it preserves the Onsager symmetry of transport coefficient [3, 12].

C. Temperature Change

We now evaluate the material derivative of temperature. To this end, we treat the internal energy as a function of species densities and temperature, $e = e(\{\rho\}, T)$. Then

$$\dot{e} = \sum_i \left(\frac{\partial e}{\partial \rho_i}\right)_{\{\rho\}_i,T} \dot{\rho}_i + \left(\frac{\partial e}{\partial T}\right)_{\{\rho\}} \dot{T}, \tag{39}$$

where $\{\rho\}_i$ is the set of all densities with ρ_i being excluded. Using Eq. (3) and (4) we obtain

$$C_V \left[\frac{dT}{dt}\right]_{irr} = \sum_i \left(\frac{\partial e}{\partial \rho_i}\right)_{\{\rho_i\}',T} (\nabla \cdot J_i) - \frac{1}{\rho} (\nabla \cdot J_e), \tag{40}$$

where we omitted the reversible hydrodynamic terms in the r.h.s., and so we obtain not the complete material derivative of temperature, but only its irreversible component, hence $[.]_{irr}$ in the l.h.s. The specific constant-volume heat capacity is denoted by $C_V = \left(\frac{\partial e}{\partial T}\right)_{\{\rho\}}$. The mass and energy fluxes are given by Eqs. (34) and (35), respectively. The obtained expression does not include the chemical transformation rates R_i explicitly and is therefore applicable it the two opposite limits of very slow and very fast chemistry. In the former case, the expression is applied literally. In the latter case, it is also applicable but the function $e = e(\{\rho\}, T)$ has to be understood in a way that $\{\rho\}$ is only constraining the elemental densities and the actual energy is evaluated at densities resulting from the complete chemical equilibration of $\{\rho\}$ at temperature T.

An important application of Magpie is to produce an EOS for a system with fixed elemental abundances and very fast chemical equilibration. Under these conditions, EOS can be written as

$$P = P(\rho, e), \tag{41}$$

where ρ is the total density. Such EOS, generated by Magpie, is applicable in problems of chemical decomposition of HE, where the chemistry is coupled to hydrodynamics [14]. In such cases, since the elemental abundances are assumed fixed, it is convenient to treat the mixture of products as an effectively single-component fluid, i.e., not keeping track of local densities of chemical species ρ_i, just like in Eq. (41). Such single-component treatment is however generally impossible when transport is present, since the mass transport can change elemental abundances locally. Ignoring the mass transport on the level of EOS, i.e., ignoring the variation of elemental abundances, might lead to inaccuracies but generally preserve conservation laws. However, the heat conduction for a single-component system cannot be generally written as the Fourier's law $\rho C_V \left[\frac{dT}{dt}\right]_{irr} = \nabla \cdot (\kappa \nabla T)$ since there are multiple terms with spatial derivatives in Eq. (40) and it is generally impossible to rewrite them exactly as a single divergence operator of some vector field. The problem with this is that the divergence in the Fourier's law guarantees the energy conservation, which would not be preserved generally if we combine Eq. (40) with the assumption of the single-component system, that is if the local elemental abundances are assumed invariant. One possibility to fix the energy preservation and to still assume a single-component system is to set J_i to zero in Eq. (40). However, this might lead to physically inconsistent situations since for example just setting $J_i = 0$ in Eq. (10) does not generally preserve positivity of the local entropy production in Eq. (32). The simplest (but not necessarily the most accurate) way of combining the requirements of (i) positivity of entropy production, (ii) single component assumption, and (iii) the Fourier's law form of Eq. (40) is to assume that the local equilibration with respect to mass transport is established much faster than the local equilibration with respect to energy transport. Then, for any given X_e one finds X_i so that J_i vanishes in Eq. (34). The result of this is that the entropy production is still positive since no terms are omitted in Eq. (10), some of them just vanish in a physically consistent manner because of the specific relationship between X_e and X_i, and Eq. (40) reduces to

$$\rho C_V \left[\frac{dT}{dt}\right]_{irr} = -\nabla \cdot J_e, \tag{42}$$

which is exactly of the Fourier's law form. Writing this expression more explicitly produces

$$\rho C_V \left[\frac{dT}{dt}\right]_{irr} = -\nabla \cdot \left[\sum_i L_{ei} X_i' + L_{ee} X_e\right], \tag{43}$$

where X_i' is not an independent mass force, but, as mentioned above, is found by solving the following system of linear equations

$$0 = J_i = L_{ie} X_e + \sum_j L_{ij} X_j'. \tag{44}$$

This system of equations is under-defined because $\sum_i J_i = 0$ is always the case. From the perspective of X'_j, we see that if it satisfies the equations, then $X'_j + \delta$ also satisfies it since $\sum_j L_{ij} = 0$. On the other hand, this freedom in X'_j does not affect the energy flux since $J_e = L_{ee}X_e + \sum_i L_{ei}X'_i$ does not change upon the substitution $X'_j \to X'_j + \delta$ since $\sum_i L_{ei} = 0$. To properly solve the system we can always add an additional equation $\sum_i X'_i = 0$ and solve the resulting system of equations using the singular value decomposition. The solution of this problem can be expressed as $X'_i = M_i X_e$. Then we have

$$\rho C_V \left[\frac{dT}{dt}\right]_{irr} = \nabla \cdot \left[\frac{L_{ee} + \sum_i L_{ei}M_i}{T}\nabla T\right], \tag{45}$$

and, therefore, the effective single-component thermal conductivity is

$$\kappa_\infty = \frac{L_{ee} + \sum_i L_{ei}M_i}{T}. \tag{46}$$

In an arbitrary equilibrium system where the temperature gradient is "turned on" instantaneously at $t = 0$ and maintained constant at $t > 0$, the mass fluxes are present transiently due to the thermal diffusion but then vanish at $t \to \infty$ when concentration gradients have set up. The energy flux at large times is, therefore, exactly the one determined by Eqs. (45) and (46), and so the subscript of κ_∞ refers to the $t \to \infty$ regime [3].

Eq. (46) can also be written for the case where iDOF are not accounted for to produce $\kappa_\infty^{(E)}$. It is convenient to express κ_∞ through $\kappa_\infty^{(E)}$. To this end, we take Eq. (28) without the second r.h.s term since all the mass fluxes vanish for κ_∞

$$J_e = J_e^{(E)} + T\sum_i c_i D_i \rho_i X_e. \tag{47}$$

Since $J_e = -\kappa_\infty \nabla T$ and $J_e^{(E)} = -\kappa_\infty^{(E)}\nabla T$, we obtain

$$\kappa_\infty = \kappa_\infty^{(E)} + \sum_i c_i D_i \rho_i. \tag{48}$$

For a single-component gas this formula is equivalent to the improved Eucken correction, Eq. (11.2-20) in Ref. **(author?)** [5]. The obtained expression is very convenient because it allows us to calculate $\kappa_\infty^{(E)}$ and D_i directly from the pure (i.e., without iDOF) Enskog theory and then calculate κ_∞ using c_i obtained from Magpie.

IV. RESULTS AND DISCUSSION

We start this section by demonstrating how to calculate transport properties of a static binary mixture with no iDOF. The mixture is static in a sense that there is no chemical equilibration and the molar fractions of chemical species are independent of pressure and temperature. The molar masses of the two species are 18 g/mol and 44 g/mol, and the mixture is 1 : 1 by moles. Here, and in what follows the notation $x : y$ will always be used to specify mixture by moles (and not by weight), so that the molar fractions are $\frac{x}{x+y}$ and $\frac{y}{x+y}$. The two options for the molecular diameters are (i) constant PT-independent hard sphere diameters of 2.65 Å and 3.3 Å chosen to approximately represent H_2O and CO_2, respectively [8], and (ii) the effective molecular diameters for H_2O and CO_2, obtained in Magpie with the use of the Ross variational perturbation theory [13, 14]. The constant hard sphere diameters and Ross effective diameters, evaluated at $T = 3000\,\mathrm{K}$(chosen arbitrarily) within a range of total densities, are depicted by solid and dashed lines, respectively, in the left panel of Fig. 1.

The right panel of Fig. 1 gives the pressure of the mixture as a function of density. The solid line represents the pressure of the constant-diameter hard spheres, evaluated with the Carnahan-Starling EOS (CS-EOS) [4, 10], implemented as a part of the Enskog transport module. The dashed line is the pressure obtained in Magpie from the Ross theory. At large densities corresponding to packing fractions ~ 1, the system transitions to a condensed phase (solid phase for constant-diameter hard spheres [6]), and the pressure starts diverging rapidly with density. Fig. 2 shows the dependence of a set of linearly independent RET transport coefficients on density. All the other transport coefficients can be restored using the general matrix properties of $L_{ij}^{(E)}$ and $L_{1e}^{(E)}$ discussed in Sec. II. Specifically, for the binary mixture one has $L_{11}^{(E)} = -L_{12}^{(E)} = -L_{21}^{(E)} = L_{22}^{(E)}$ and $L_{1e}^{(E)} = L_{e1}^{(E)} = -L_{2e}^{(E)} = -L_{e2}^{(E)}$. Other properties, in the form of inequalities, follow from the semi-definiteness of the matrix of transport coefficients

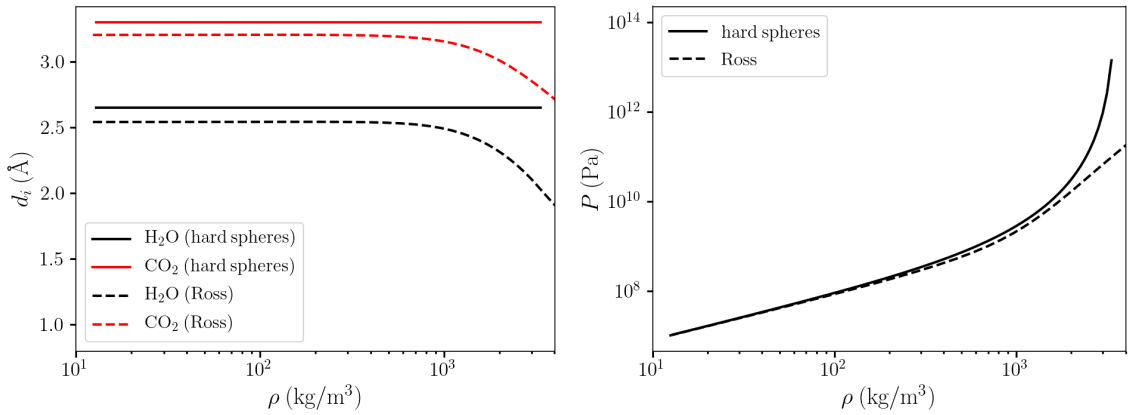

Figure 1. (left) Molecular diameters in the $1:1$ mixture of H_2O and CO_2 at $T = 3000\,\mathrm{K}$. (right) Pressure of the mixture at the same temperature is evaluated with CS-EOS for constant-diameter hard spheres (solid black line) and with the Ross perturbation theory (dashed black line).

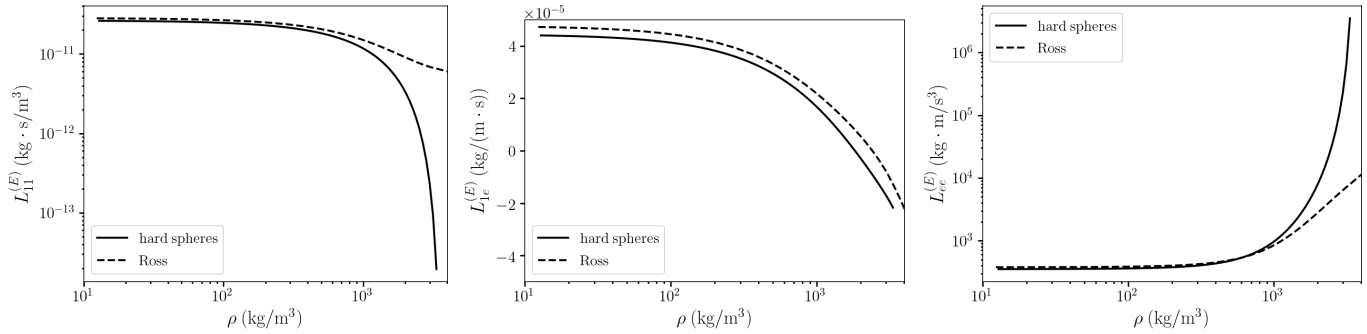

Figure 2. Pure Enskog transport coefficients for the $1:1$ mixture of H_2O and CO_2 at $T = 3000\,\mathrm{K}$.

in Eq. (11). Specifically, it dictates that $L_{ii}^{(E)}, L_{ee}^{(E)} \geqslant 0$ [3], which is what is observed in the left and right panels. The inequalities for $L_{ie}^{(E)}$ are more complex [3]

$$L_{ii}^{(E)} L_{ee}^{(E)} \geqslant \left[L_{ie}^{(E)}\right]^2, \tag{49}$$

and so these coefficients can change sign as is exemplified in the middle panel.

The dependence of the transport coefficients on density could be quite involved. We consider the situation where the temperature is constant, i.e., $X_e = 0$, and so Eq. (5) becomes

$$\begin{aligned} J_1 &= L_{11}^{(E)}(X_1 - X_2), \\ J_2 &= L_{11}^{(E)}(X_2 - X_1), \\ J_e &= L_{1e}^{(E)}(X_1 - X_2). \end{aligned}$$

At low densities, i.e., in the almost-ideal gas situation, the mass and energy fluxes are dominated by the component of the mixture with the lowest molecular mass (the first component in our case), since its molecules are fastest. It can be demonstrated that $X_i \propto -\nabla\rho_i$ for the ideal gas and since, physically we must have $J_1 \propto -\nabla\rho_1$ and $J_e \propto -\nabla\rho_1$, we conclude that the both $L_{11}^{(E)}$ and $L_{1e}^{(E)}$ are to be positive at low densities ($L_{11}^{(E)}$is in fact positive at any density, as discussed above). This prediction agrees with what is seen in the left two panels of Fig. 2.

At large densities, the chemical potentials of the components grow very quickly and diverge at a finite density for the CS-EOS [4]. Accordingly, the magnitude of X_i could become very large. On the other hand, the material fluxes must vanish under these conditions since the hard spheres jam above the fluid-to-solid phase transition. This leads to a prediction that $L_{ij}^{(E)}$ drop quickly at large densities which is indeed what is seen in the left panel of Fig. 2. The

energy flux does not vanish even when the hard spheres jam, since the energy is transferred by molecular collisions of adjacent molecules. Under these conditions, what is expected to dominate the energy transport is the component with the larger excluded volume (the second component in our case), because this is the molecules of this component that jam and, therefore, transfer energy effectively through the "jammed lattice". Therefore, it is expected that $J_e \propto -\nabla\rho_2$ and since $X_2 \propto -\nabla\rho_2$, we predict that $L_{1e}^{(E)}$ becomes negative at large densities [11], in agreement with the numerical results in the middle panel of Fig. 2.

With regards to $L_{ee}^{(E)}$, it was already discussed that it must always stay non-negative. More can be said about its dependence on density with the help of Eq. (49). The coefficient $L_{1e}^{(E)}$ is observed to change not too rapidly at large densities in middle panel of Fig. 2, whereas $L_{11}^{(E)}$ drops quickly in the left panel of the same figure. Setting $i = 1$ in Eq. (49) produces $L_{11}^{(E)} L_{ee}^{(E)} \geqslant \left[L_{1e}^{(E)}\right]^2$, and so $L_{ee}^{(E)}$ has to grow rapidly with density to satisfy this inequality at rapidly decaying $L_{11}^{(E)}$. This expected rapid growth is indeed observed in the right panel of Fig. 2.

The self-diffusion coefficients for the two chemical species are given in the leftmost panel of Fig. 3. Since it

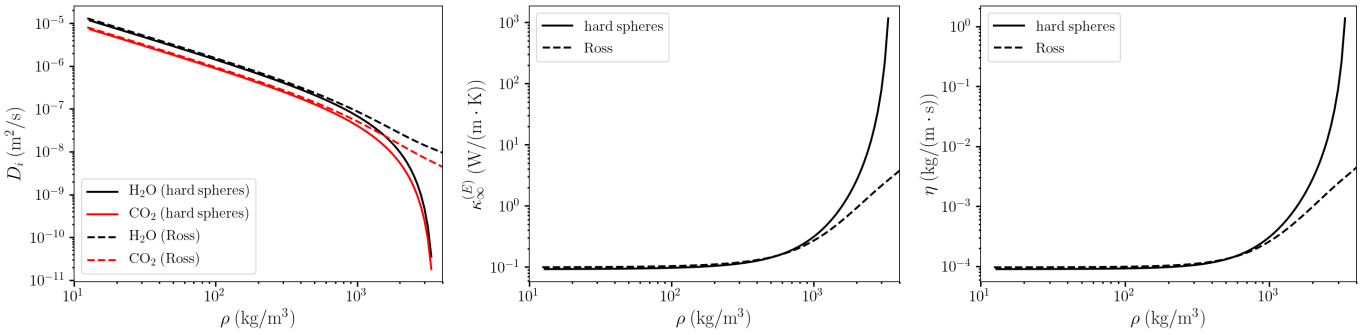

Figure 3. (left) Self-diffusion coefficients, (middle) thermal conductivity, and (right) the dynamic viscosity for the 1 : 1 mixture of H_2O and CO_2 at $T = 3000\,\mathrm{K}$.

describes the mass transport, it decays rapidly with density when the system undergoes gas-to-fluid/solid transition. The dependence of the thermal conductivity $\kappa_\infty^{(E)}$, Eq. (46), on density is shown in the middle panel of Fig. 3. At large densities, where L_{ei} is small, Eq. (46) reduces to $\kappa_\infty = L_{ee}/T$, and so the middle panel of Fig. 3 and the rightmost panel of Fig. 2 look very similar. The dynamic viscosity η is plotted in the rightmost panel of Fig. 3 and is seen to grow rapidly with density at large densities. The values for the thermal conductivity and the viscosity at $P = 20\,\mathrm{GPa}$ ($\rho \approx 1.8\,\mathrm{g/cm}$) are $\kappa_\infty^{(E)} \approx 1.67\,\mathrm{W/(m \cdot K)}$ and $\eta \approx 1.8 \times 10^{-3}\,\mathrm{kg/(m \cdot s)}$, respectively, which is consistent with the results of molecular dynamics simulations and Enskog calculations in Ref. [1].

A. Including iDOF

Fig. 4 shows the results for the same 1 : 1 mixture of Magpie's H_2O and CO_2, where the effect of iDOF is included. The dashed lines give the pure Enskog (i.e., no-iDOF) results, and so the dashed lines in the left and middle panels

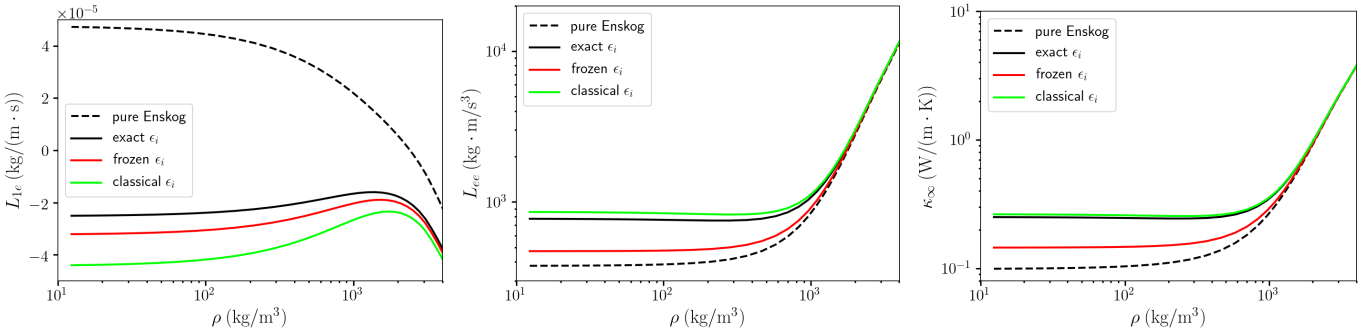

Figure 4. Transport coefficients L_{1e} and L_{ee}, and thermal conductivity κ_∞ for the 1 : 1 mixture of H_2O and CO_2 at $T = 3000\,\mathrm{K}$.

are exactly those previously plotted in the middle and right panels of Fig. 2. The solid lines in all the three panels correspond to the full transport coefficients and conductivity. Specifically, the full transport coefficients L_{1e} (left panel) and L_{ee} (middle panel) are evaluated with Eqs. (37) and (38), respectively. The full thermal conductivity κ_∞ in the right panel is calculated with Eq. (48). The solid black lines represent the case where the iDOF energy of a molecule is given by

$$\epsilon = \epsilon^{(0)} + \frac{\xi}{2} k_B T + \sum_{i=1}^{n_{vib}} k_B \theta_i \left[e^{\theta_i / T} - 1 \right]^{-1}, \tag{50}$$

where the first term is the molecular energy at zero temperature, and the second term is the free-rotation contribution with the number of rotational degrees of freedom $\xi = 3$ and $\xi = 2$ for H_2O and CO_2, respectively. The third term is the contribution of the intra-molecular vibrations, each described by a quantum harmonic oscillator with the "Einstein temperature" θ_i and the zero-point energy excluded, so that this contribution vanishes at $T = 0$. At low temperatures ($T \ll \theta$), this last contribution is exponentially small. The transport coefficients evaluated with the vibrational contribution set to zero (i.e., the case of a "frozen" quantum harmonic oscillator) is shown by the solid red lines. On the other hand, the solid green lines represent the results of calculations where the last term is substituted by what it reduces to in the high-temperature classical limit, $\sum_{i=1}^{n_{vib}} k_B \left[T - \theta_i / 2 \right]$.

The rightmost panel of Fig. 4 shows the dependence of $\kappa_\infty^{(E)}$ on total density. First, it is seen that accounting for iDOF change the result significantly. The difference between classical and exact quantum formulations of intramolecular energy (green and black lines) is not too large because of the relatively high temperature. At lower temperatures (e.g., $T < 1000$, not shown) this difference becomes more pronounced since the vibrations become more quantum mechanical, thus rendering the classical approximation less accurate. It has to be noted however that the energy flux J_e can be counter-intuitive, especially when there is chemical equilibration. In particular, in this case the total energy shift $\epsilon^{(0)}$ in Eq. (50) is rather arbitrary and, for example, it is always possible to shift the energy so that there is energy flux from cold to hot. Such energy flux would not contradict the thermodynamics, however, as the entropy production would stay non-negative and this energy flux would mostly be because of the "cold" energy of the molecule - it stays with the molecule so the heat (as opposed to energy) would still flow from hot to cold.

It can be noted here that the results for exact Eq. (50) are noticeably different from the both "classical" and "frozen" ones. This is important because it means that at considered temperatures classical molecular dynamics, or even quantum molecular dynamics will not be very accurate since they treat vibrational motions classically.

Fig. 5 shows the result of transport calculations for $H_2O(g)$ where the chemical equilibration is performed with respect to the dissociation reaction

$$2H_2O(g) \rightleftarrows 2H_2(g) + O_2(g). \tag{51}$$

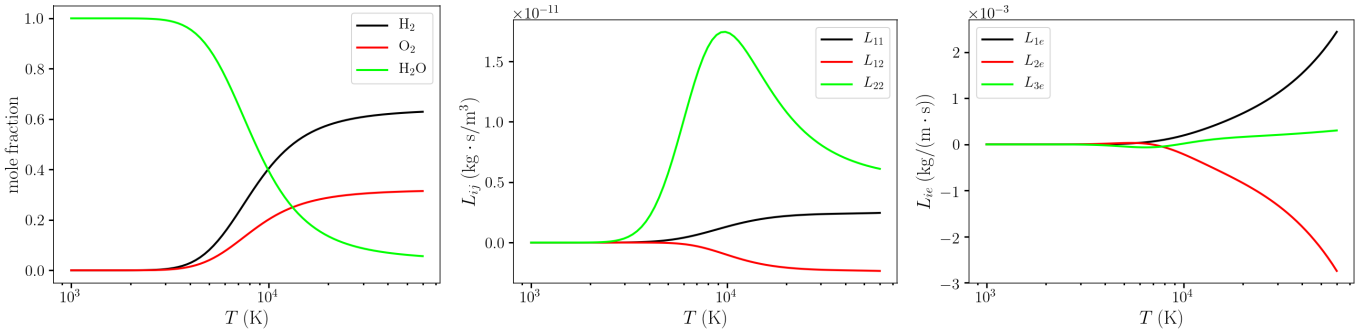

Figure 5. The dependence of the full transport coefficients on temperature for the chemically equilibrated mixture, Eq. (51), at $P = 1\,\mathrm{GPa}$. Species' indices of 1, 2 and 3 in the last two panels correspond to H_2, O_2 and H_2O, respectively.

The transport calculations are performed at $P = 1\,\mathrm{GPa}$ in a range of temperatures. As is seen in the leftmost panel, the chemical equilibrium in Eq. (51) is strongly shifted towards $H_2O(g)$ at low temperatures. Under these conditions, the gas becomes effectively mono-component and so L_{ij} and L_{ie} vanish. At higher temperatures, all the three components are present. The sum of the three L_{ie} coefficients vanish exactly because of the symmetry of the transport coefficients. Of all the nine transport coefficients L_{ij}, only three are linearly independent. Our choices for the three linearly independent coefficients, L_{11}, L_{12} and L_{22}, are plotted in the middle panel.

Fig. 6 shows the translational chemical potentials, $\mu_i^{(tr)}$ in Eq. (30), evaluated for the $1:1$ mixture of H_2 and O_2 gases at $T = 3000\,\mathrm{K}$ in a range of total mixture densities. Chemical potentials are plotted multiplied by molar masses

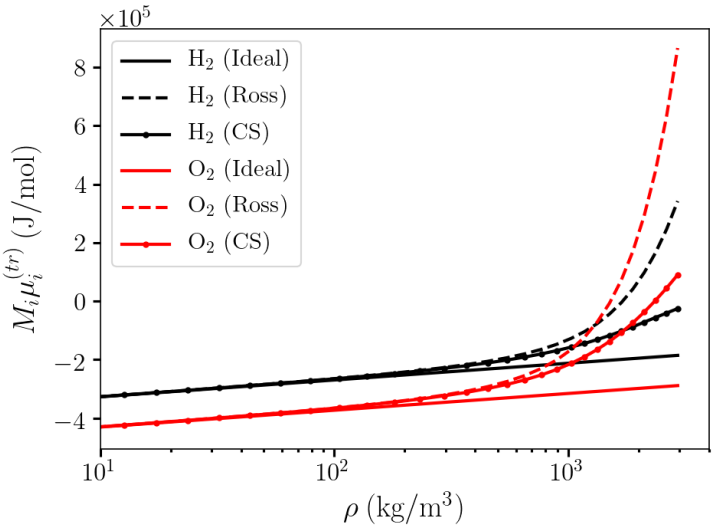

Figure 6. Comparison of translational chemical potentials, assuming the ideal gas, Ross perturbation theory, and CS-EOS, for the 1 : 1 mixture of H_2 (black lines) and O_2(red lines) at $T = 3000\,\mathrm{K}$.

M_i to give the molar chemical potentials. The translational chemical potentials for the ideal mixture of ideal gases, $M_i\mu_i^{(tr,\mathrm{ideal})} = RT \ln\left[\frac{\rho_i}{m_i}\left(\frac{2\pi\hbar^2}{m_i k_B T}\right)^{3/2}\right]$, are plotted by solid lines and are seen to agree well (up to $\rho \sim 10^2\,\mathrm{kg/m^3}$) with dashed lines, which represent the Ross theory, as implemented in Magpie. The results for the CS-EOS, plotted by solid lines with small filled circles, are seen to agree with the Ross results up to $\rho \sim 10^3\,\mathrm{kg/m^3}$. At low densities the molar chemical potential of oxygen is lower than that of hydrogen since oxygen molecules are heavier and, therefore, more "classical" at the same temperature, i.e., the density of quantum-mechanical states is higher and so the entropy is also higher. At very high densities, the chemical potential of oxygen becomes larger than that of hydrogen because of the larger effective hard-sphere diameter of the former.

When evaluating energy and material fluxes with the Enskog theory, one needs to find the gradient of the chemical potentials to evaluate the mass forces, Eq. (6). Presumably, the most accurate of the chemical potentials in Fig. 6 is the one calculated with the Ross theory. However, the particular implementation of the Enskog theory **(author?)** [4, 9] was developed for constant-diameter hard spheres, and, in particular, relied on the CS-EOS when evaluating certain parameters of the pair distribution functions. Therefore, for consistency we suggest using CS-EOS to evaluate the chemical potentials of chemical species in gas/fluid mixtures. Employing more accurate EOS, e.g., the Ross theory, directly within the Enskog theory is typically referred to as "modified Enskog theory" which, however, might have internal consistency problems, see discussion in Ref. [1] and references therein. We do not discuss nor use the "modified Enskog theory" in this work and use the CS-EOS to evaluate $\mu_i^{(tr)}$ in the calculations in the next subsection.

B. HMX decomposition

In this subsection we consider the energy transport in a situation which, very approximately and qualitatively (but not quantitatively), mimics the flame structure in HMX [15]. To this end, we assume that the temperature profile in the flame is given by a rescaled and shifted error function so that the characteristic flame thickness is $\sim 1\,\mathrm{mm}$, and the temperature span is from 700 K to 5000 K. This assumed temperature profile is shown in the left panel of Fig. 7. At each pressure and temperature, the mass fractions of "HMX decomposition products" N_2, H_2O, CO_2, CO, NO, H_2, O_2 and $CH_4$are calculated by minimizing the Gibbs free energy of their mixture subject to the HMX stoichiometry $C_4H_8N_8O_8$. The Gibbs free energy minimization is performed using Magpie [14] as a Python library. The resulting mass fractions at $P = 0.01\,\mathrm{GPa}$ are given in the right panel of Fig. 7.

The reason we need an actual temperature profile is that we want to see the effect of including the contributions of iDOF on the on the efficiency of energy transfer. The energy flux J_e by itself does not provide a convenient perspective since it inherently includes such significant contributions as the energy flux due to "cold" and zero-point energies of molecules which of course is a legitimate contribution, but it does not change local temperature. We, therefore, choose to calculate the temperature growth rate, given by Eq. (40), and see how this rate depends on inclusion of various

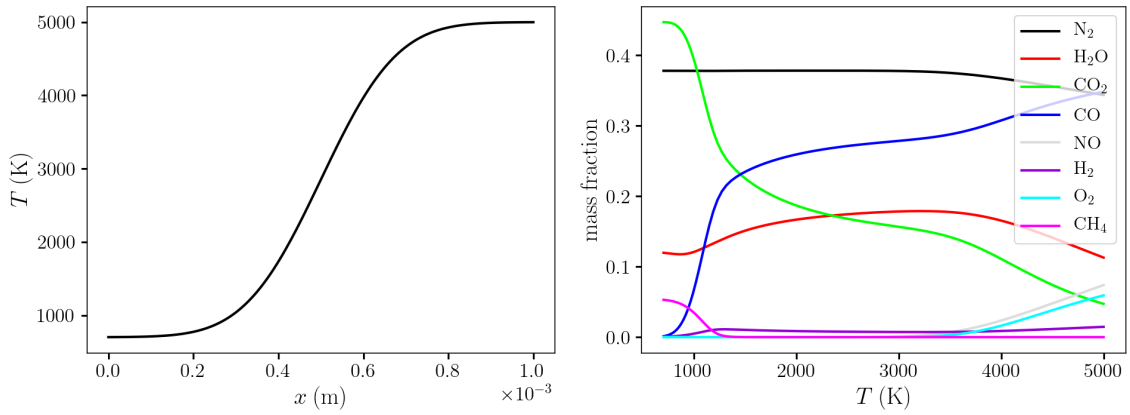

Figure 7. (left) Temperature profile used in the energy transport calculations. (right) Mass fractions of $C_4H_8N_8O_8$ decomposition products at $P = 0.01\,\mathrm{GPa}$.

contributions to the energy and mass fluxes. Since Eq. (40) depends not only on the first, but also on second spatial derivatives of temperature (through terms like ∇X_e), choosing a smooth spatial profile for temperature is a natural (but of course not unique) way to provide a link between temperature and its first and second spatial derivatives. The black line in the left panel of Fig. 8 shows the result of evaluation of Eq. (40) with all its r.h.s terms included. The red line gives the result where the first r.h.s term (the one with $\nabla \cdot J_i$) is neglected in Eq. (40), so it acquires the

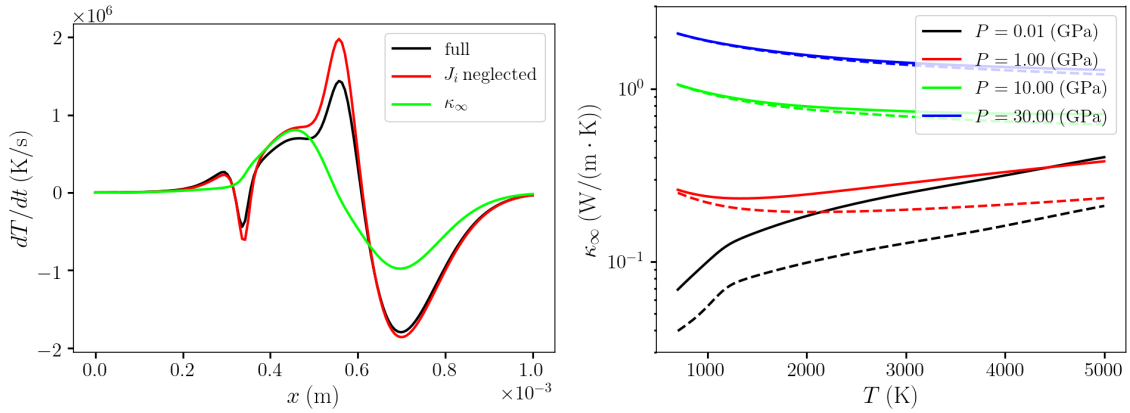

Figure 8. (left) Temperature growth rate due to the energy and mass transports within the "HMX flame" profile depicted in the left panel of Fig. 7. (right) Thermal conductivity of the mixture of HMX decomposition products as a function of temperature for several different pressures. Solid and dashed lines correspond to κ_∞ and $\kappa_\infty^{(E)}$, respectively, in Eq. (48).

Fourier's law form, which is essential for hydrodynamics calculations if the concentration of all the chemical species is not explicitly tracked. The both black and red curves are seen to be not too different, demonstrating an overall smooth behavior except for a dip at $x \sim 0.3\,\mathrm{mm}$ and a spike at $x \sim 0.6\,\mathrm{mm}$. From the left panel of Fig. 7, these two peculiarities can be seen to correspond to $T \approx 1000\,\mathrm{K}$ and $T \approx 4000\,\mathrm{K}$, respectively. These two temperatures correspond to where the mass fractions vary substantially with temperature in the right panel of Fig. 7. Because of these variations, the gradients of concentrations of species are large at those two temperature, resulting in substantial mass fluxes, which contribute to the temperature growth rate. The exclusion of the J_i-based first r.h.s. term in Eq. (40) does not make those peculiarities disappear since J_i also contributes to J_e when iDOF contributions are accounted for, as is clear from Eq. (28). It is also important to remind here that even though the exclusion of the first r.h.s term in Eq. (40), which resulted in the red line in the left panel of Fig. 8, might seem preferable from the hydrodynamic standpoint because of the acquired Fourier's law form, such exclusion is not thermodynamically consistent. Indeed, J_i is excluded only partially since its contribution to J_e in Eq. (28) remains. Such partial exclusion does not guarantee the positive entropy production in Eq. (32) and is, therefore, potentially dangerous. Instead, the complete exclusion of J_i can be performed in a physically consistent manner, as described at the end of Subsection III C. The result of

this exclusion, leading to introduction of the thermal conductivity κ_∞, is shown in left panel of Fig. 8 by the green line. Even though this line lacks the previously observed peculiarities, related to large concentration gradients of chemical species, it still provides a reasonable approximation to the full result, given by the black line. Therefore, in a situation where the concentration of separate species is not explicitly tracked in hydrodynamic simulations, the last approach is preferred because of its internal physical consistency.

The right panel of Fig. 8 shows the thermal conductivity as the function of temperature along four representative isobars. The full thermal conductivity κ_∞ and the pure Enskog one $\kappa_\infty^{(E)}$ are represented by the solid and dashed lines, respectively. At high pressures (i.e., packing fraction ~ 1), material fluxes and self-diffusion are strongly suppressed and therefore the non-translational contributions are small [1], as is evidenced by the small difference between the solid and dashed blues lines, $P = 30\,\mathrm{GPa}$. However, the contribution of the iDOF to the thermal conductivity could be of the same order of magnitude as the translational one at lower pressures (black and red lines in the right panel of Fig. 8), and therefore cannot be ignored.

V. CONCLUSION

In conclusion we provide the algorithm for how to calculate the transport properties of a mixture:

1. Magpie EOS is obtained for a mixture, for example $1:1$ mixture of H_2O and CO_2, in Magpie. The mixture can be chemically equilibrated or not. In the former case the "input mixture" serves merely to set the overall elemental abundances and the actual concentrations of species could be different and pressure- and temperature-dependent (for example H_2, O_2 and CO could be produced in appreciable amounts for the discussed mixture of water and carbon dioxide).

2. The effective hard sphere diameters are calculated inside the Magpie EOS. This value could be extracted by an auxiliary function provided with the Enskog library.

3. These diameters, along with the species concentrations (chemically equilibrated or not) and the molecular masses are used to evaluate the pure Enskog transport coefficients $L_{ij}^{(E)}$, $L_{ie}^{(E)}$, $L_{ee}^{(E)}$, self-diffusion coefficients D_i and, for example, viscosity.

4. Pure Enskog transport coefficients and the self-diffusion coefficients are then used, together with iDOF energies ϵ_i (obtained from an auxiliary function from the Enskog library) to evaluate the full transport coefficients with Eqs. (37) and (38).

5. To now evaluate the energy and mass fluxes, one has to calculate the transport forces. The "energy" force is given by Eq. (7). The "mass" force is evaluated with Eq. (6), where the full chemical potential is given by Eq. (30).

6. We suggest calculating the translational part of the chemical potential with the CS-EOS, even though it is also available from the supposedly more accurate Magpie EOS. This is because the particular implementation of the Enskog theory for mixtures [4, 9] relies internally on CS-EOS, and, therefore, using chemical potentials from other sources might lead to physical inconsistencies.

7. The same function in the Enskog library, that calculates the pure Enskog transport coefficients, also calculates $\kappa_\infty^{(E)}$. Eq. (48) is then used to calculate the thermal conductivity κ_∞, which accounts for iDOF.

ACKNOWLEDGMENTS

Funding from Dan Borovina through the LANL "CHE Grand Challenge" Project is gratefully acknowledged. I am thankful to Jeff Leiding for multiple discussions on transport, Magpie and the manuscript.

Appendix A: Relationship between $L_{ie}^{(E)}$, $L_{ij}^{(E)}$ and $L_{\alpha e}^{(E)}$, $L_{\alpha\beta}^{(E)}$

We consider the case similar to Sec. III where within each chemical species i one can distinguish multiple subspecies, so greek letters α, β are in fact multi-indices that enumerate both chemical species and subspecies within. We assume that the collisional properties are only dependent on what chemical species are colliding, and are independent of the

specific subspecies. Under this conditions, it is expected that the transport coefficients $L^{(E)}_{\alpha e}$ and $L^{(E)}_{\alpha\beta}$ can be expression via $L^{(E)}_{ie}$, $L^{(E)}_{ij}$. In this section we consider two specific cases which will allow us to establish such relationships.

The first case corresponds to a system where there is no equilibration of the iDOFs, and p_α do no vary spatially even though ρ_i are allowed to very spatially. Under these conditions, since transport properties cannot distinguish between different subspecies of the same chemical species, p_α remains the same over time, which of course requires $J^{(E)}_\alpha = p_\alpha J^{(E)}_{c(\alpha)}$. More explicitly, this equation is

$$L^{(E)}_{\alpha e} X_e + \sum_\beta L^{(E)}_{\alpha\beta} X^{(E)}_\beta = p_\alpha \left[L^{(E)}_{c(\alpha)e} X_e + \sum_j L^{(E)}_{c(\alpha)j} X^{(E)}_j \right]. \tag{A1}$$

Since p_α does not vary spatially, Eq. (25) results in $X_\alpha = X_{i(\alpha)}$, and so the above equation transforms into

$$L^{(E)}_{\alpha e} X_e + \sum_\beta L^{(E)}_{\alpha\beta} X^{(E)}_{c(\beta)} = p_\alpha \left[L^{(E)}_{c(\alpha)e} X_e + \sum_j L^{(E)}_{c(\alpha)j} X^{(E)}_j \right]. \tag{A2}$$

Since this equation has to remain identity at arbitrary X_e and $X^{(E)}_i$, one has the following relations

$$L^{(E)}_{\alpha e} = p_\alpha L^{(E)}_{c(\alpha)e},$$
$$\sum_{\beta\in j} L^{(E)}_{\alpha\beta} = p_\alpha L_{c(\alpha)j}.$$

The second case is a system where temperature and the densities of molecular species are spatially invariant, but p_α vary spatially. Under these conditions, the mass transport for a subspecies can be written as

$$J^{(E)}_\alpha = -D_{c(\alpha)} \nabla \rho_\alpha = -D_{c(\alpha)} \rho_{c(\alpha)} \nabla p_\alpha, \tag{A3}$$

which serves as the definition of D_i - the self-diffusion coefficient of species i. On the other hand, the same flux can be written as $J^{(E)}_\alpha = \sum_\beta L^{(E)}_{\alpha\beta} X^{(E)}_\beta$. For the system considered we have $X^{(E)}_i = 0$, and so this expression transforms into

$$J^{(E)}_\alpha = -\sum_\beta L^{(E)}_{\alpha\beta} \frac{k_B T}{m_{c(\beta)}} \frac{\nabla p_\beta}{p_\beta}. \tag{A4}$$

Since this is the same flux, we have

$$D_{c(\alpha)} \rho_{c(\alpha)} \nabla p_\alpha = \sum_\beta L^{(E)}_{\alpha\beta} \frac{k_B T}{m_{c(\beta)}} \frac{\nabla p_\beta}{p_\beta}. \tag{A5}$$

This equation has to remain identity at arbitrary local values of p_α and their gradients, as long as $\sum_{\alpha\in i} p_\alpha = 1$ and $\sum_{\alpha\in i} \nabla p_\alpha = 0$. Mind however that $L^{(E)}_{\alpha\beta}$ is a function of p_α (but not of ∇p_α).

Eq. (A5) suggests a way to evaluate self-diffusion coefficients if we have a computer code to evaluate $L^{(E)}_{\alpha\beta}$. The simplest way to do that is to "split" a chemical species i into two subspecies a and b so that $p_a + p_b = 1$ and $\nabla p_a + \nabla p_b = 0$. All the other species are not split into subspecies, and therefore $p_\alpha = 1$ and $\nabla p_\alpha = 0$ for $c(\alpha) \neq i$. Then, Eq. (A5) can be transformed to

$$D_i = \frac{k_B T}{m_i \rho_i} \left(\frac{L^{(E)}_{aa}}{p_a} - \frac{L^{(E)}_{ab}}{p_b} \right). \tag{A6}$$

Transport coefficients $L^{(E)}_{aa}$ and $L^{(E)}_{ab}$ are functions of p_a and p_b in such a way that the resulting D_i does not depend on their choice as long as $p_a + p_b = 1$.

---

[1] S. Bastea. Transport properties of fluid mixtures at high pressures and temperatures, application to the detonation of hmx. In *12th Symposium (International) on Detonation.*

[2] S. Chapman and T. G. Cowling. *The Mathematical Theory of Non-Uniform Gases*. Cambridge University Press, 3 edition, 1995.
[3] S. R. De Groot. *Thermodynamics of Irreversible Processes*. North-Holland, Amsterdam, 1951.
[4] J. J. Erpenbeck. Transport coefficients of hard-sphere mixtures: Theory and monte carlo molecular-dynamics calculations for an isotopic mixture. *Phys. Rev. A*, 39(9):4718–4731, 1989.
[5] J. H. Ferziger and H. G Kaper. *Mathematical Theory of Transport Processes in Gases*. North-Holland Publishing Company, Amsterdam, 1972.
[6] J. P. Hansen and I. R. McDonald. *Theory of Simple Liquids*. Academic Press, London, 1986.
[7] J. O. Hirschfelder. Heat conductivity in polyatomic or electronically excited gases. ii. *J. Chem. Phys.*, 26(2):282–285, 1957.
[8] A. F. Ismail, K. C. Khulbe, and T. Matsuura. *Gas Separation Membranes: Polymeric and Inorganic*. Springer International Publising, 2015.
[9] M. Lopez de Haro, E. G. D. Cohen, and J. M. Kincaid. The enskog theory for multicomponent mixtures. i. linear transport theory. *J. Chem. Phys.*, 78(5):2746–2759, 1983.
[10] G. A. Mansoori, N. F. Carnahan, K. E. Starling, and T. W. Leland. Equilibrium thermodynamic properties of the mixture of hard spheres. *J. Chem. Phys.*, 54:1523–1525, 1971.
[11] The two proportionality relations were derived in the ideal gas limit and unlikely to be accurate at large densities. However, the signs in them are expected to be correct on physical grounds, which is sufficient for obtaining the sign of $L_{1e}^{(E)}$.
[12] L. Onsager. Reciprocal relations in irreversible processes. i. *Phys. Rev.*, 37(4):405–426, 1931.
[13] M. Ross. A high-density fluid-perturbation theory based on an inverse 12th-power hard-sphere reference system. *J. Chem. Phys.*, 71(4):1567–1571, 1979.
[14] C. Ticknor, S. A. Andrews, and J. A. Leiding. Magpie: a new thermochemical code. *AIP Adv.*, (accepted), 2020.
[15] M. J. Ward, S. F. Son, and M. Q. Brewster. Steady deflagration of hmx with simple kinetics: A gas phase chain reaction model. *Comb. Flame*, 114:556–568, 1998.